Int. J. Electrochem. Sci., 9 **(2014)** 5974 - 5992

International Journal of
ELECTROCHEMICAL
SCIENCE
www.electrochemsci.org

Multi-component Olivine for Lithium-Ion Hybrid Capacitor

Manickam Minakshi[1,*], *Shanmughasundaram Duraisamy*[2], *Penki Rao Tirupathi*[2], *Sathiyaraj Kandhasamy*[1] *and Munichandraiah Nookala*[2,*]

[1]Department of Chemistry, Murdoch University, Murdoch, WA 6150, Australia
[2]Inorganic and Physical Chemistry, Indian Institute of Science, Bangalore 560012, India
[*]E-mail: minakshi@murdoch.edu.au; muni@ipc.issc.ernet.in

Received: 5 June 2014 / *Accepted:* 6 August 2014 / *Published:* 25 August 2014

A lithium-ion hybrid capacitor comprising of a battery type multi-component olivine ($LiMn_{1/3}Co_{1/3}Ni_{1/3}PO_4$) cathode and a capacitive type carbon negative electrode is reported. Olivine phosphate synthesized with chelating agent's polyvinylpyrrolidone (PVP) or triethanolamine (TEA) showed uniform carbon coating through in-situ process exhibiting a surface area 5.1 m^2/g with porosity 0.02 cm^3/g. The surface area for commercial carbon electrode was observed to be 1450 m^2/g with high porosity 0.76 cm^3/g. Galvanostatic charge/discharge cycling tests were conducted in the coin cells, olivine vs. Li, offering a cell voltage of 4.75 V vs. Li with a maximum specific capacitance of 125 F/g. In the case of olivine vs. carbon in a lithium-ion hybrid device delivered a high discharge capacitance of 86 F/g at a specific current of 0.12 A/g with a cycling retention of 53 F/g (38% loss) after 250 cycles. The obtained performance of PVP synthesized olivine material is manifested to uniform carbon coating and the trapped organic products that provide pathways for facile electrochemical reactions than their TEA counterparts.

Keywords: Olivine; Lithium-ion; Hybrid; Capacitor; Polymer; Carbon; Porosity.

1. INTRODUCTION

Among the available electrochemical energy storage devices, i.e. batteries, fuel cells and supercapacitors, the supercapacitors are known for their high power densities and longer life time exhibiting high coulombic efficiency [1]. Supercapacitors (also called electrochemical capacitors) store energy in two parallel electrodes with opposing charges using one of the mechanisms either ion adsorption (electrochemical double layer capacitor, EDLC) formed at electrode/electrolyte interface or fast surface redox reactions (pseudo-capacitors) between the electrode and the electrolyte [1-3]. In contrast to EDLC, pseudocapacitors store charge faradaically through electron transfer between electrode and electrolyte achieving through insertion and extraction processes [4-5]. The

electrochemical capacitors are considered as excellent storage device that compliment batteries, as the primary requisite for these devices in providing quick charge release when required and the amount of charge they can accommodate is not as crucial as for batteries [2-3, 6]. These devices are used to deliver a high power during a short time in combination with rechargeable lithium batteries, resulting in hybrid devices with high specific energy and high specific power that could be suitable for applications such as electric vehicles and large-scale stationary energy storage and conversion [7]. In the past two decades, numerous publications have appeared on various electrode materials that have been investigated for battery and capacitor system as a single electrode [8-17]. However, either the current battery technologies or symmetric capacitor system alone cannot meet large scale applications due to poor efficiency and power density. To meet these requirements, in recent years, an "asymmetric" energy storage device has been developed with capacitive electrodes of different natures. Very recently, hybrid device relating to a distinct charge storage mechanism with the combination of battery type and capacitor-like electrode has also been developed [18-19].

The term "asymmetric" means different electrochemical active materials with different operating potentials as positive and negative electrodes that increase the overall cell potential, resulting in higher energy and power densities [18-19]. Asymmetric hybrid capacitors (also called hybrid capacitors) reported in the literature include a range of combinations of electrode materials such as conducting polymer vs. carbon [20], conducting polymer vs. metal oxide [21], carbon vs. metal nitrides [22], carbon vs. metal oxides [23], carbon vs. metal phosphates [24].

Following the oxide based intercalants, a technological breakthrough has occurred, using phosphates as host in rechargeable battery systems. It has been reported that the materials based on the tetrahedral polyanion unit (PO_4) are structurally more stable than those of the oxide counterparts, MnO_2 and $LiCoO_2$ [10]. In this context, lithium iron phosphate ($LiFePO_4$) has been widely studied as a lithium insertion host for a decade now [10] which demonstrated the reversible intercalation and de-intercalation of lithium and found suitable for rechargeable battery applications. The success of $LiFePO_4$ as a cathode material for a battery system inspired the present investigation on the lithium (multi-component transition metal) phosphate compound and extending this for a potential application in hybrid devices. The reported olivine-type $LiCoPO_4$ for hybrid device in a non-aqueous media didn't exhibit the long term cycleability [25]. The alternative, $LiNiPO_4$, has safety and cost issues associated with poor cycling stability [26-27]. Hence, in the present work, the combination of Mn, Co and Ni phosphate (multi-component olivine cathode; $LiMn_{1/3}Co_{1/3}Ni_{1/3}PO_4$) as a host compound has been investigated to tune the redox couple of the transition metal cations present.

The aim of the current work is to investigate the cathode material with the new multi transition metal lithium phosphate that can sustain high rate performance and be able to maintain large capacitance after multiple cycles. To the best of our knowledge, multi-component olivine of this combination $LiMn_{1/3}Co_{1/3}Ni_{1/3}PO_4$ has not been studied in hybrid devices using non-aqueous solutions. However, in a separate study, this compound has been tested for aqueous battery system and those results have been reported by us elsewhere [28]. Also, a multi-component olivine type of $LiMn_{1/3}Co_{1/3}Fe_{1/3}PO_4$ has been reported by Kang et al [29] and used as a cathode for lithium secondary batteries exhibiting an excellent performance. In the current work, we have adopted a sol-gel synthetic route to prepare $LiMn_{1/3}Co_{1/3}Ni_{1/3}PO_4$ using chelating agents such as polyvinylpyrrolidone (PVP) and

triethanolamine (TEA) and have evaluated its capacitance performance vs. Li metal. For hybrid device configuration, a commercial carbon has been used as anode in non-aqueous electrolyte, 1M $LiPF_6$ dissolved in ethylene carbonate, diethyl carbonate and dimethyl carbonate (2:1:2 v/v). Carbon has been chosen as EDLC electrode owing to its high surface area, low cost, porosity and chemically stability with wide range of operating temperatures.

2. EXPERIMENTAL

Sol–gel synthesis of $LiCo_{1/3}Mn_{1/3}Ni_{1/3}PO_4$ was performed while mixing a stoichiometric amount of precursors containing lithium acetate, cobalt acetate, manganese acetate, nickel acetate, ammonium dihydrogen phosphate in distilled water with an effective stirring. During stirring, polyvinylpyrrolidone (PVP) was added to the solution as a chelating agent in 1:1 weight ratio to the metal ions. The pH of the solution was adjusted to 3.5 by adding nitric acid. The resulting sol was then heated at 80 °C for an hour to obtain a viscous gel. Then, the thick transparent gel was dried at 110 °C in hot air oven for 12 h. The resultant powder was calcined at 300 °C for 8 h and at 550 °C for 6 h in air with intermittent grinding. The resultant furnace cooled "olivine" powder was ground for further analysis. The carbon powder (YEC8) used in this study was "as-received" form purchased from Fuzhou Yihuan Carbon Co., China.

The synthesized olivine lithium phosphate ($LiMn_{1/3}Co_{1/3}Ni_{1/3}PO_4$) powders were subject to systematic physical and electrochemical studies. Powder X-ray diffraction (XRD) patterns were recorded on a X-ray diffractometer (Bruker D8 advance diffractometer) with a Cu Kα radiation (λ = 1.5418 Å) source. The microscopy studies were carried out using a scanning electron microscopy (FEI Co. Sirion) and transmission electron microscopy (JEOL JEM 2100F). Surface area and pore size distribution of the samples were measured using Micromeritics surface area analyser (model ASAP 2020).

All electrochemical studies were carried out in a coin cell (CR2032). Both the olivine and carbon powders were coated on stainless steel disc as current collector. Li metal was used as counter and reference electrodes. The stainless steel disc was polished with successive grades of emery, degreased, etched in dilute 10% HNO_3 and 10% HCl, washed with detergent and rinsed with distilled water and acetone followed by drying in air. The active material (olivine, 75 wt %), conductive material (Ketjen black, 15 wt %) and polyvinylidene fluoride (PVDF, 10 wt %) were mixed and ground in a mortar. In the case of carbon electrode, conductive material wasn't included in the preparation. Few drops of n-methyl pyrrolidinone (NMP) were added to form slurry. The slurry was coated on the pre-treated stainless steel foil until getting the required loading level and dried the coated disc at 100 °C under reduced pressure for 12 h. A non-aqueous solution of 1M $LiPF_6$ dissolved in ethylene carbonate, diethyl carbonate and dimethyl carbonate (2:1:2 v/v) electrolyte (Chameleon) was used as an electrolyte. The cyclic voltammetry (CV) and galvanostatic charge-discharge cycling were measured by a Biologic SA multichannel potentiostat/galvanostat model VMP3.

3. RESULTS AND DISCUSSION

The sol-gel method is a wet-chemical synthetic technique that has attracted special interest [30] and used widely for the fabrication of materials whose morphologies range from discrete particles to continuous polymer networks [31]. Its importance will be evident from the capacitance measurements as detailed in the following section. Generally, sol-gel preparation involves hydrolysis and polycondensation reactions of metal ion precursors that pave the way to synthesize organic – inorganic nanocomposites. The distinct advantage of using this methodology as opposed to the conventional solid-state sintering is that, obtaining a porous material through gel process, control of grain growth and achieving the resultant product at a much lower temperature [32]. Here, polymer assisted method (polyvinylpyrrolidone (PVP) and triethanolamine (TEA)) is used for the production of higher surface area nanocomposites as well as for preventing particle aggregation.

3.1 Physical Characterization

3.1.1 XRD diffraction studies

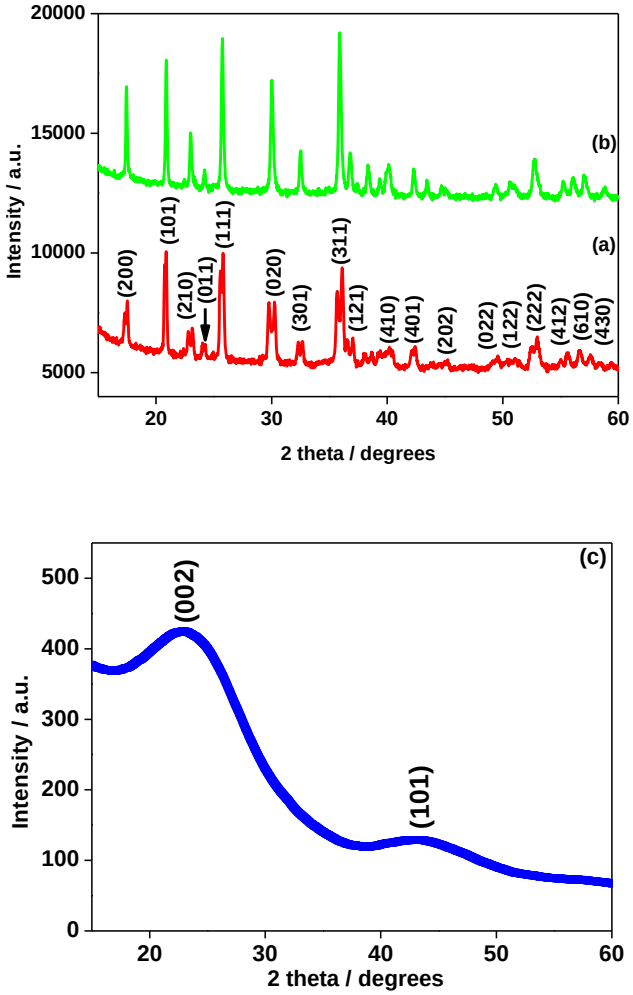

Figure 1. X-ray diffraction (XRD) patterns of as-synthesized multi-component olivine $LiMn_{1/3}Co_{1/3}Ni_{1/3}PO_4$ samples with chelating agents (a) PVP and (b) TEA with hkl indexes of major reflection peaks marked, (c) represents the pattern for as-received carbon powder.

Powder X-ray diffraction (XRD) patterns of the as-synthesized olivine $LiMn_{1/3}Co_{1/3}Ni_{1/3}PO_4$ material with the chelating agent PVP and TEA are displayed in Fig. 1(a-b), respectively. All diffraction peaks in Fig. 1a-b are indexed to multi-component olivine cathode i.e. $LiMn_{1/3}Co_{1/3}Fe_{1/3}PO_4$ [29] and pure olivine structure (orthorhombic) with *Pmna* space group (PDF 01-085-0002) of the parent $LiFePO_4$ compound [33]. As the combination of multi dopant cations (Mn, Co and Ni) have a comparable ionic radius the material is preferred to crystallize identical to lithium iron phosphate compound. The observed diffraction patterns are identical to that reported for multi-component olivine cathode by Kang et al [29]. The sharp diffraction peaks with high intensity indicate that the as-synthesized olivine material is a well crystalline and the chosen sol-gel process is very effective to prepare new polymer inorganic material at a low temperature (550° C) synthetic route. A small peak splitting is observed in the major diffraction peaks obtained for PVP as the chelating agent (Fig. 1a) which is a characteristic of the chosen chelating agent. This can be explained by the formation of discrete olivine phases such as $LiMnPO_4$, $LiCoPO_4$ and $LiNiPO_4$ [34-35]. The existence of these multiple single phase compounds with slightly varying lattice parameter led to splitting in major peaks. Triethanolamine as the chelating agent reacts with dopant cations and acts as a surfactant during the synthesis [36]. Furthermore, it is also suggested that adsorption of TEA residue on the surface of the olivine powders may have controlled the peak splitting (Fig. 1b) and its morphology. The role of the chelating agent is that above the decomposition temperature, the chelating agent decomposes and the carbon atoms are then entangled in the PVP capped $LiMn_{1/3}Co_{1/3}Ni_{1/3}PO_4$ with a uniform coating layer on the surface [37]. Despite this, no carbon-related diffraction peaks could be detected, this suggests that the carbon generated from the PVP and TEA could be amorphous or too little to detect through the XRD technique. Evidently, the presence of carbon (from CHNS analysis) in the olivine materials using PVP and TEA was found to be 0.6% and 3.0% respectively. The lower amount of carbon seen in the olivine (PVP) composite illustrates PVP not only functions as a capping agent [37] to control the particle grain growth but also contributes to the effective trapping of organic layer over the active material that enhances the monodispersity between the particles [38]. The higher amount of carbon content in the olivine (TEA) composite shows TEA just acts as shape controller. Figure 1c shows the XRD pattern of carbon powder with broad peaks illustrating an amorphous in nature. The absence of (004) and (006) peaks (in Fig. 1c) indicates the type of carbon is non-graphitic.

3.1.2 Microscopy studies : SEM and TEM

To study the role of PVP and TEA and its effect on the shape, size, morphology, porosity and particle aggregation of $LiMn_{1/3}Co_{1/3}Ni_{1/3}PO_4$ synthesized by sol-gel route, the as-prepared samples have been subjected to a range of microscopy analysis and the results are displayed in Figs. 2-6. Figure 2 shows SEM images of (a-b) olivine materials synthesized by PVP and (c-d) TEA as well as (e-f) carbon.

It can be observed from Fig. 2 (a-d) that the materials mainly consist of well defined particles in submicron range (0.1 – 0.3 μm). The dispersion and strong binding of metal ions by PVP and TEA, allows the high degree of interparticle contacts and densification, which are prerequisites for energy

storage materials. The XRD results are in parallel with SEM corroborating the strong crystallinity of the as-synthesized olivine materials.

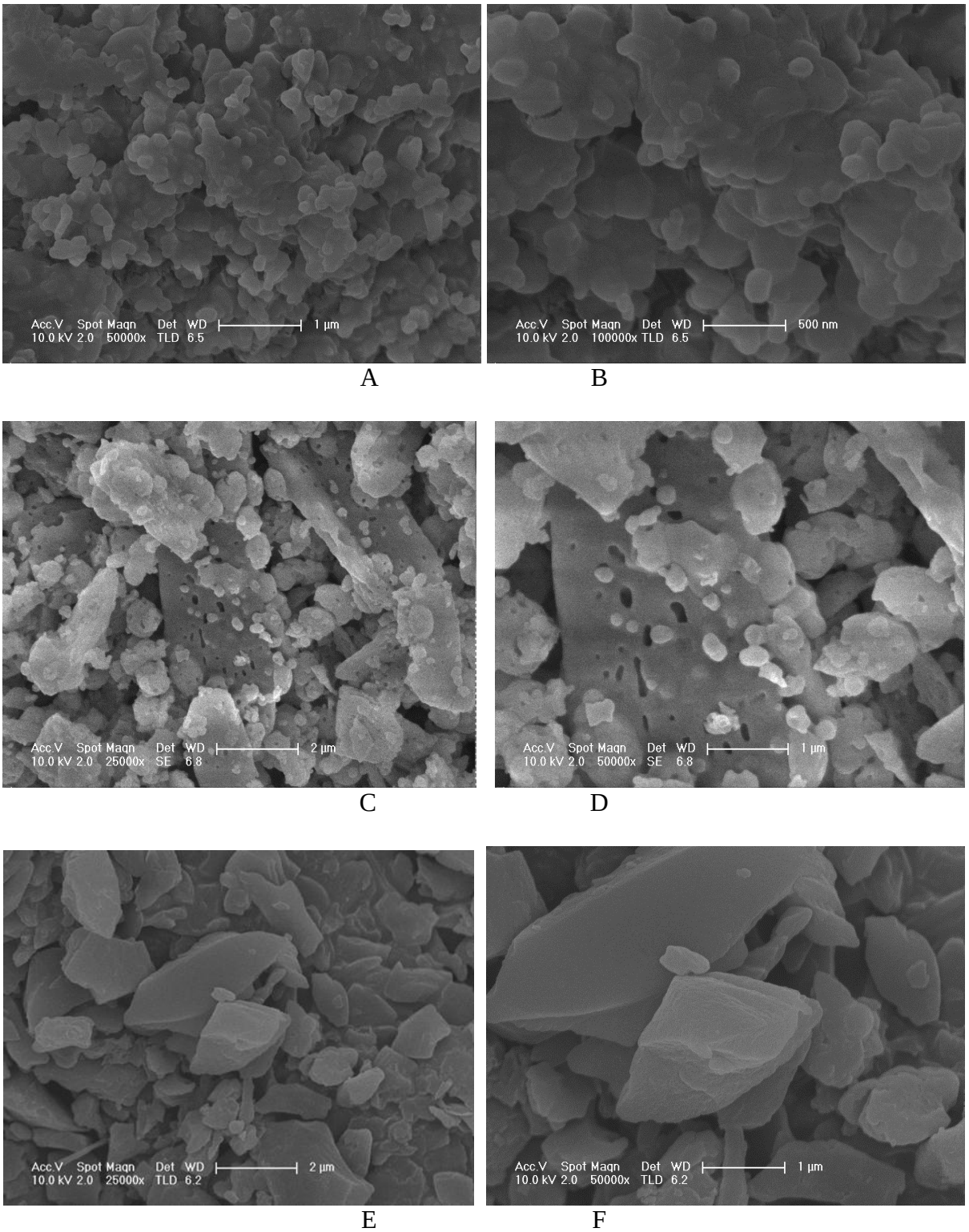

Figure 2. Scanning electron micrographs (SEM) of as-synthesized multi-component olivine $LiMn_{1/3}Co_{1/3}Ni_{1/3}PO_4$ samples with chelating agents (a-b) PVP and (c-d) TEA with different magnifications. Images (e-f) represents as-received carbon powder with different magnifications.

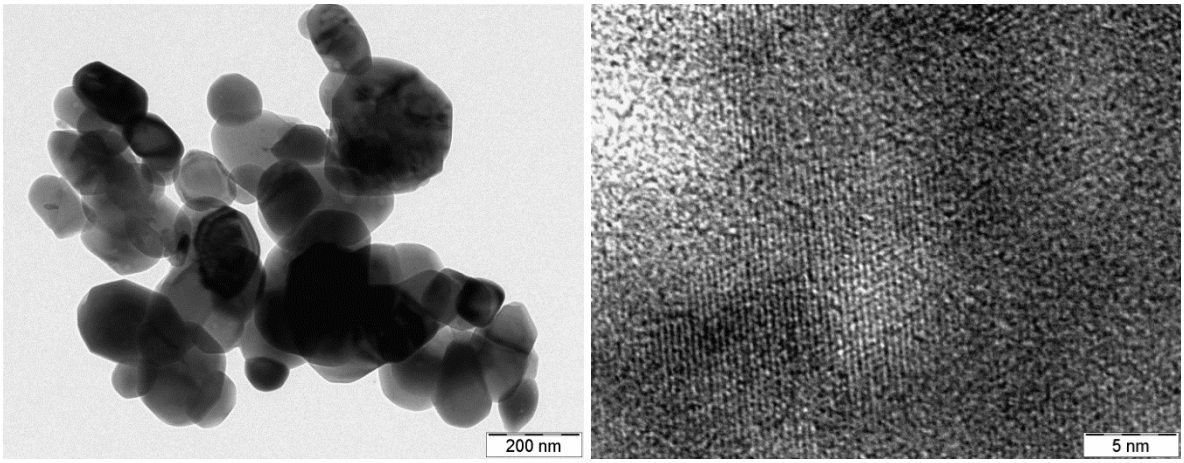

A B

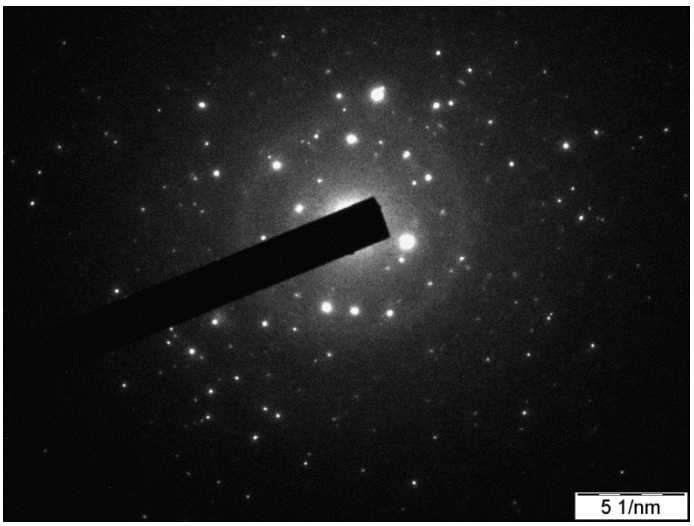

C

Figure 3. Transmission electron microscope (TEM) images of as-synthesized multi-component olivine $LiMn_{1/3}Co_{1/3}Ni_{1/3}PO_4$ samples with chelating agents PVP (a) regions showing clustered particles of good connectivity with uniform carbon coating and its maginified image, (b) showing lattice fringes of crystalline in nature and (c) corresponding selected area electron diffraction pattern (SADP) indicating a crystalline phase with good ring patterns.

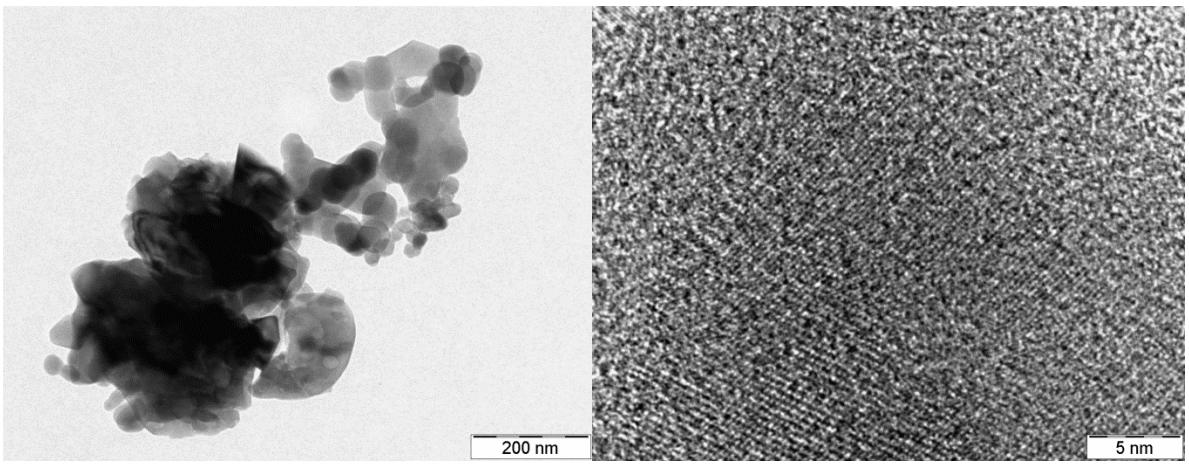

A B

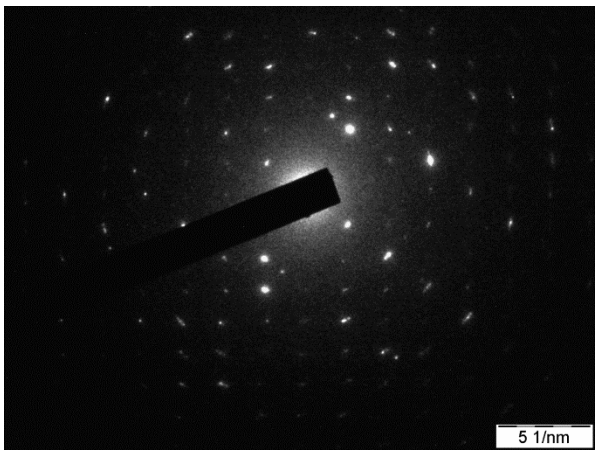

C

Figure 4. Transmission electron microscope (TEM) images of as-synthesized multi-component olivine $LiMn_{1/3}Co_{1/3}Ni_{1/3}PO_4$ samples with chelating agents TEA (a) regions showing particle morphology and size distribution and its maginified image, (b) showing lattice fringes of less crystalline in nature and (c) corresponding selected area electron diffraction pattern (SADP) with lower number of brighter spots.

The SEM images of the as-received carbon (Fig. 2 (e-f)) show plate-like stacked morphology with diameter in the range 0.2 – 2 μm. The samples are also analysed for TEM, HRTEM and SADP. From the TEM images of the olivine material with PVP (Fig. 3a-c) it is clearly seen that particles have a good interparticle contact possessing polymer matrix with uniform carbon coating [39]. In addition, these particles shows lattice fringes indicating a good crystallinity and the corresponding selected area diffraction pattern displays several concentric rings composed of individual diffraction spots, confirming the polycrystalline nature of the as-synthesized olivine material with PVP as chelating agent [39]. The TEM photographs of the olivine material with TEA (Fig. 4a-c) show aggregated fine particle size (≤100 nm). The HRTEM lattice image, in Fig. 4b, indicates less-defined crystalline regions with no clear fringes. The corresponding selected area diffraction pattern, in Fig. 4c, shows lower number of individual diffraction spots and undefined concentric ring like patterns to that of observed for PVP samples. The finer particle size means the short diffusion distance for intercalant ions.

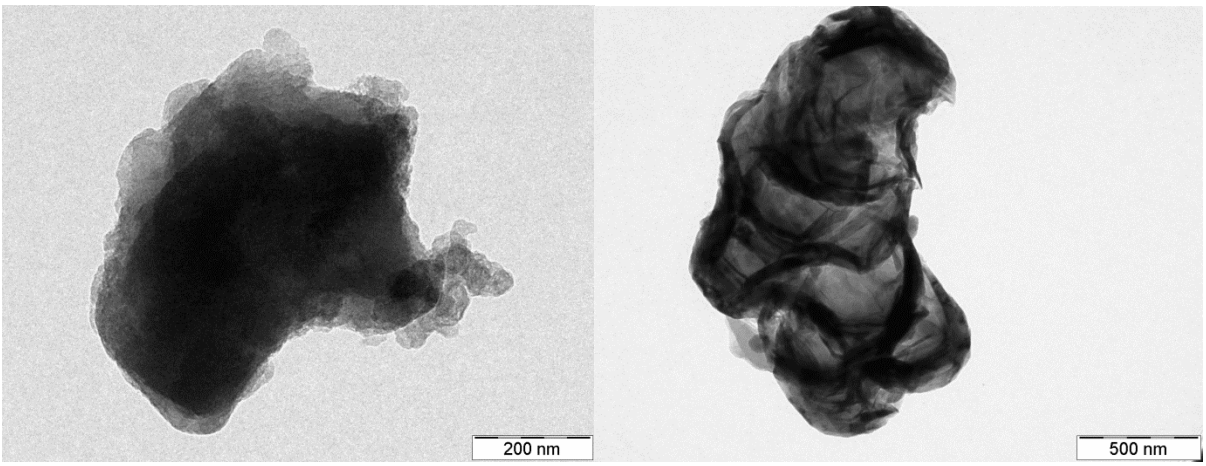

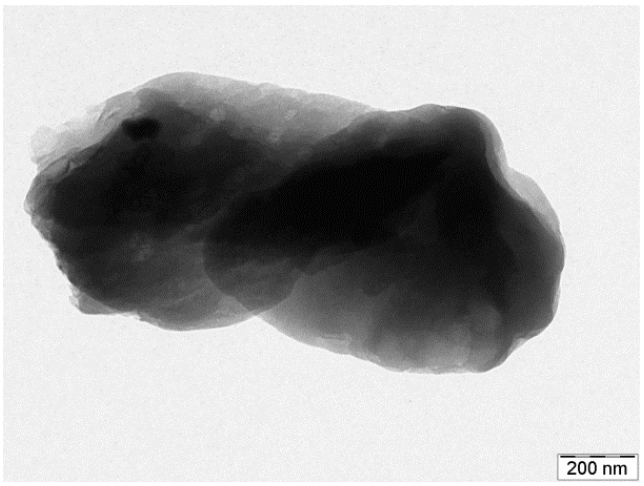

Figure 5. Transmission electron microscope (TEM) images of as-received carbon powder under different magnifications.

This shows that the physicochemical properties of the as-synthesized olivine material strongly depend on the chelating agent chosen [28], which is favouring PVP rather than TEA. The TEM photograph of the anode material carbon shows (Fig. 5b) that carbon layer had many wrinkled and folded regions. In another photograph, Fig. 5 a and c, fragment of carbon composed of many layers indicating the type of carbon material "amorphous in nature" that's been used as electrode material in this study for hybrid device.

3.1.3 Surface area measurement : BET study

The capacitance of carbon electrode is directly related to the surface area of the electrode/electrolyte interface.

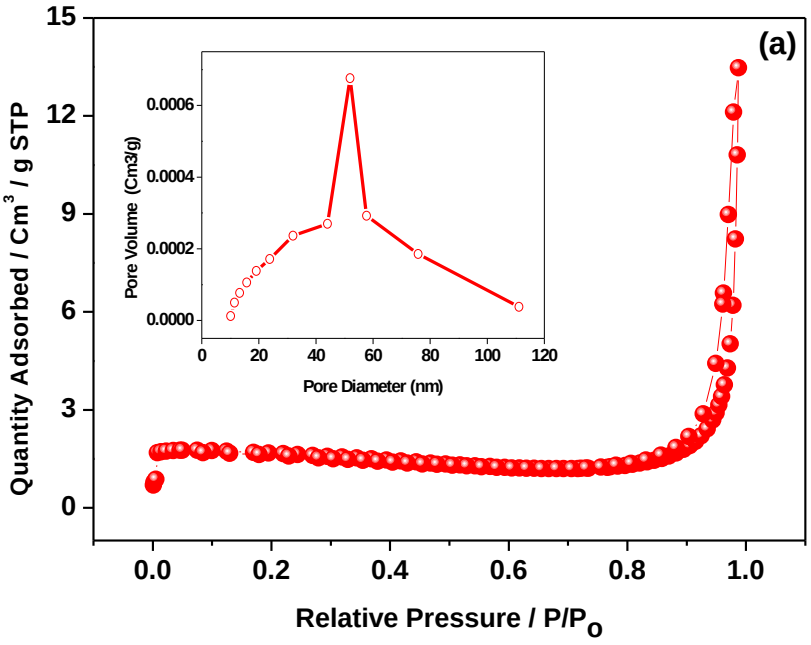

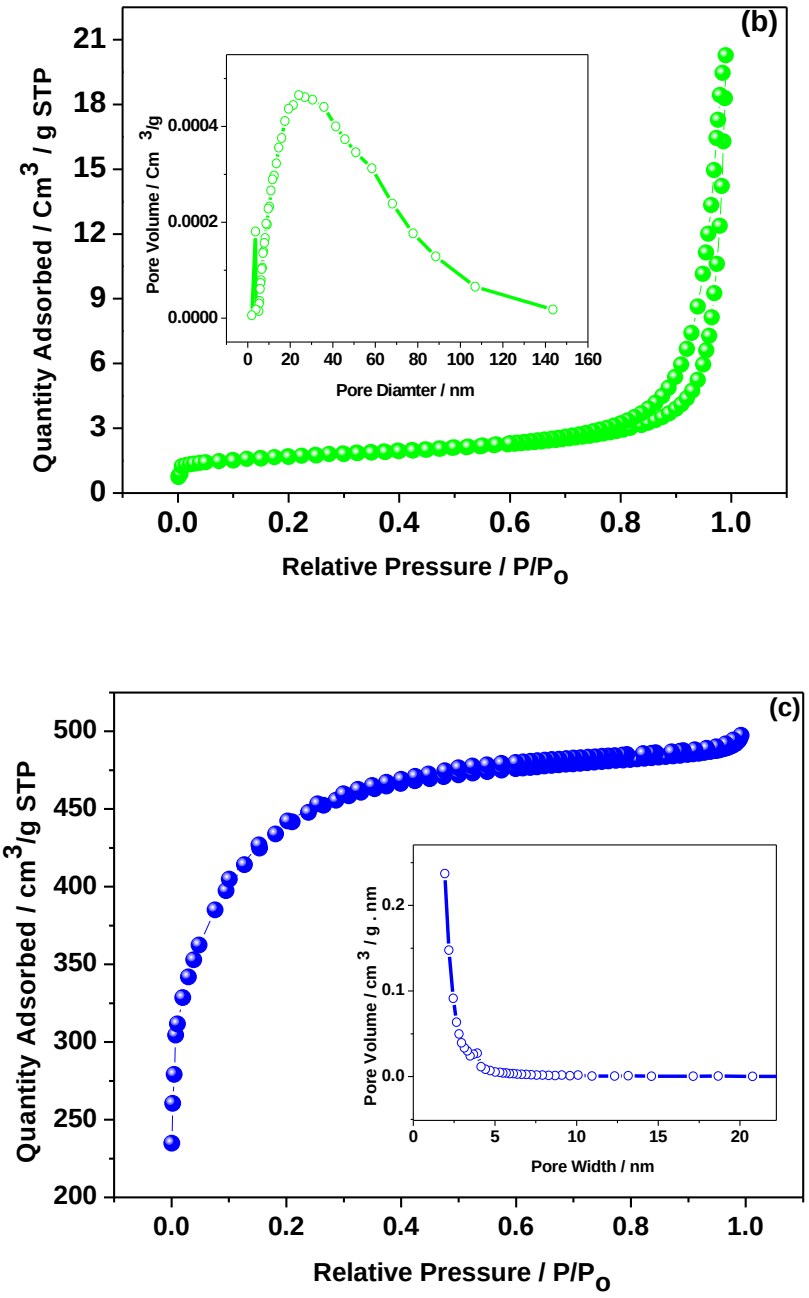

Figure 6. Nitrogen adsorption-desorption isotherms of as-synthesized multi-component olivine $LiMn_{1/3}Co_{1/3}Ni_{1/3}PO_4$ samples with chelating agents (a) PVP, (b) TEA and (c) as-received carbon powder. Pore size distributions of these composites are shown in the inset.

A relatively high specific surface area together with a narrow pore size distribution is a pre-requisite to achieve high capacitive performance in the hybrid device [40]. Hence, the Brunauer-Emmett-Teller (BET) surface area has been carried out for the electrode materials used in this study. Typical adsorption-desorption isotherms, pore volume and pore size distribution plots of the as-synthesized samples and carbon are shown in Fig. 6. The pore size distribution of the samples is calculated using the Barrett-Joyner-Halend (BJH) method.

Olivine material with PVP exhibits a narrow pore size while TEA had a broad pore size distribution of around pore diameter 20 – 60 nm. The obtained olivine material exhibits a surface area of 5.7 m^2/g and porosity 0.02 cm^3/g. The nitrogen sorption isotherms show a typical type IV isotherm with type H3 hysteresis loop and BJH plots for the samples imply the existence of mesopores. The surface area for carbon powder is observed to be 1450 m^2/g with a high porosity of 0.76 cm^3/g associated with a narrow pore size distribution and average pore size of 5 nm. Highly mesoporous material with a well developed porosity/surface area carbon coupled with olivine material used for further studies (a) could facilitate penetration of electrode/electrolyte interfacial area by providing an increase in active sites thereby led to large capacitance [41] and (b) effectively increase the physical adsorption/desorption sites of EDL capacitance [42].

3.2 Electrochemical Characterization

3.2.1 Cyclic Voltammetry : Olivine vs. metallic Li

The electrochemical performance of the olivine $LiMn_{1/3}Co_{1/3}Ni_{1/3}PO_4$ / Li and olivine $LiMn_{1/3}Co_{1/3}Ni_{1/3}PO_4$ / C hybrid device were investigated by potentiostatic and galvanostatic measurements.

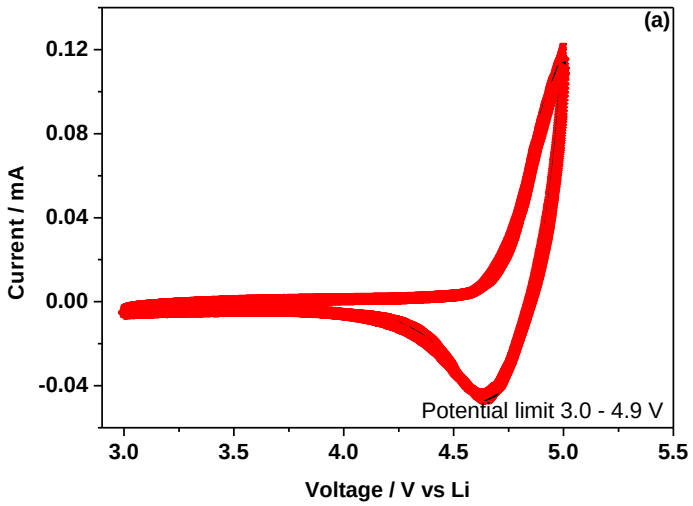

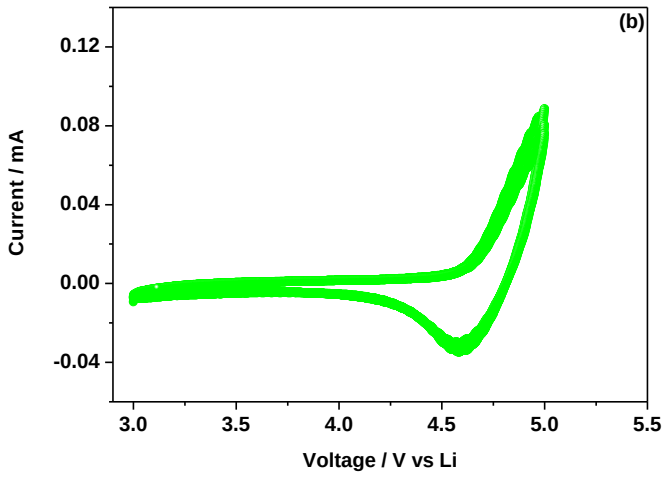

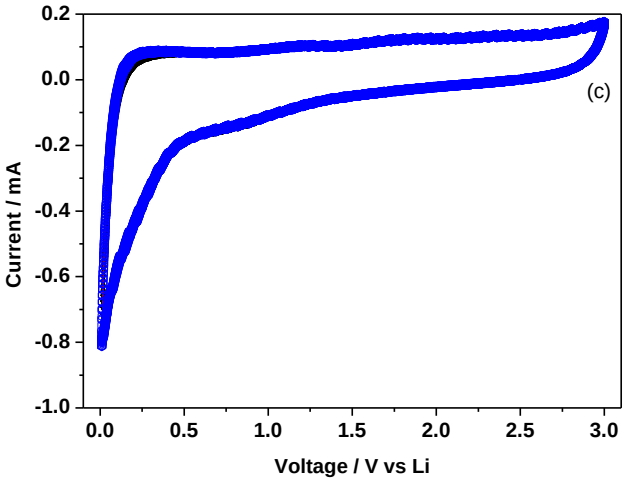

Figure 7. Cyclic Voltammogram (CV) of as-synthesized multi-component olivine $LiMn_{1/3}Co_{1/3}Ni_{1/3}PO_4$ samples with chelating agents (a) PVP, (b) TEA and (c) carbon powder versus metallic lithium in 1M $LiPF_6$ dissolved in ethylene carbonate, diethyl carbonate and dimethyl carbonate (2:1:2 v/v) non-aqueous electrolyte at a scan rate of 2 mV/s.

The capacitor was constructed with an equal mass ratio of the olivine and the carbon or lithium electrodes. The specific capacitance obtained from the charge-discharge data was calculated using the equation $C = I \cdot \Delta t / (\Delta V \cdot m)$, where *I* is the discharge/charge current imposed to the device, Δt is the time interval for the discharge/charge performance, ΔV is the potential window, and the *m* is the mass of the material.

Figure 7 shows the electrochemical performance of as-synthesized olivine electrode/Li (Fig. 7 a-b) and as-received carbon electrode/Li (Fig. 7c) at a scan rate of 2 mV/s. The cyclic voltammograms of the olivine in the voltage window 3.0 – 4.9 V vs. Li for the initial ten cycles (curves are superimposed) is shown in Figure 7a (PVP) and 7b (TEA) and a pair of redox peaks are observed clearly. As there is a stability problem of non-aqueous electrolytes around 5.0 V, the upper cut-off limit is restricted to 4.9 V. The initial scan was anodic (Li de-intercalation) and the open circuit potential was 3.02 V. The CV plots can be divided into two electrochemical processes comprising an electrical double layer (3.0 – 4.0 V) then a redox reaction (4.0 – 4.9 V). The oxidation and reduction peaks were observed at 4.9 V and 4.6 V, respectively corresponding to the Li^+ de-intercalation and intercalation behavior accessing $Co^{3+/2+}$ redox couple [33] from/into $LiMn_{1/3}Co_{1/3}Ni_{1/3}PO_4$. It appears that only the Co^{3+}/Co^{2+} redox couple is responsible for the electrochemical activity while those of Ni and Mn do not change. The presence of electrochemically inactive Ni and Mn in the multi-component olivine ($LiMn_{1/3}Co_{1/3}Ni_{1/3}PO_4$) shows only marginal performance to those reported for $LiMn_{1/3}Co_{1/3}Fe_{1/3}PO_4$ [29]. However, the CV curves of the shown multiple ten cycles remained almost unchanged in terms of peak currents, demonstrating that the electrochemical reaction is reversible in non-aqueous solutions. In addition to typical electrostatic interactions in the electrical double layer, fast faradic (redox) reactions involving electron transfer on the electrode/electrolyte interface also contributed to the charge storage processes [4]. The excellent reversibility of the multi-component

olivine material is in good agreement with the parent $LiCoPO_4$ and $LiFePO_4$ compounds [33, 43] illustrating lithium de-intercalation and intercalation processes. The overall capacitance of the olivine material is observed from both the electric double layer capacitance (non-faradaic) and the faradaic capacity generated by the redox reactions [44]. For carbon sample in the voltage window 0.0 – 3.0 V, a near rectangular, EDLC formation takes place and the process is found to be reversible for multiple cycles. The cycle showed greater cathodic currents and the observed behaviour agrees well with the reported value [45]. Hence, on the basis of these potentiostatic results, the olivine electrode reveal the typical intercalation behaviour as dominant and capacitive behaviour (capacity generated by non-faradaic reactions [46-47]) as dominant for carbon electrode within the potential range 3.0 – 4.9 V and 0 – 3.0 V respectively.

3.2.2 Galvanostatic (charge-discharge) studies: Olivine vs. metallic Li

Figure 8a-c shows the charge-discharge profiles for olivine (PVP and TEA) and carbon, respectively.

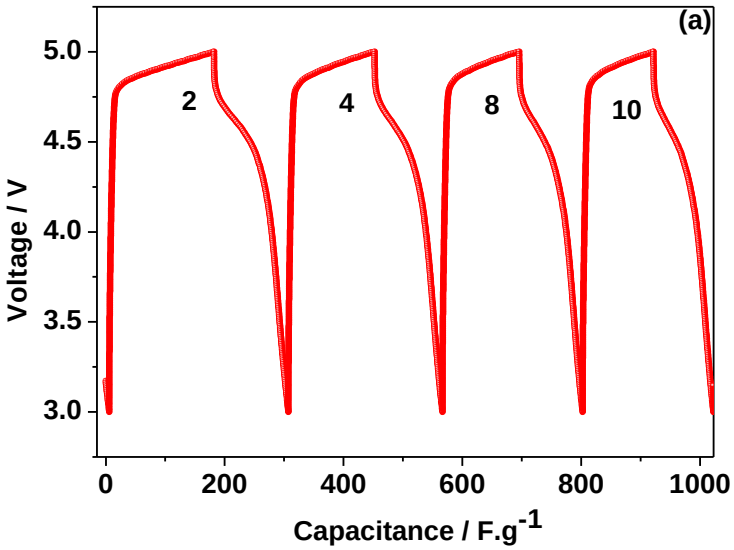

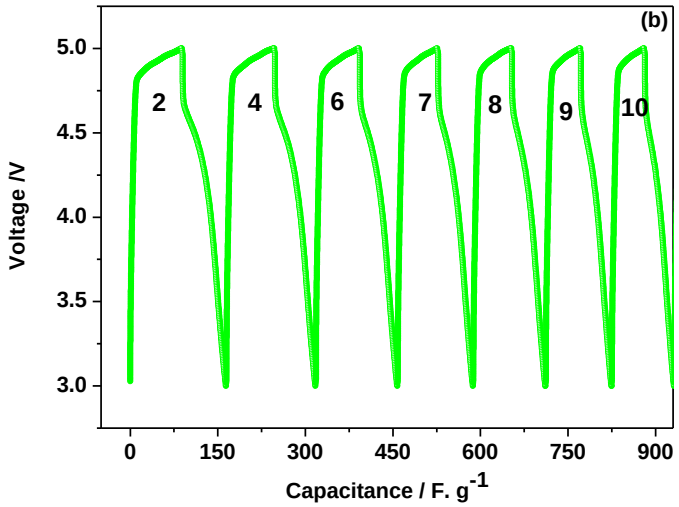

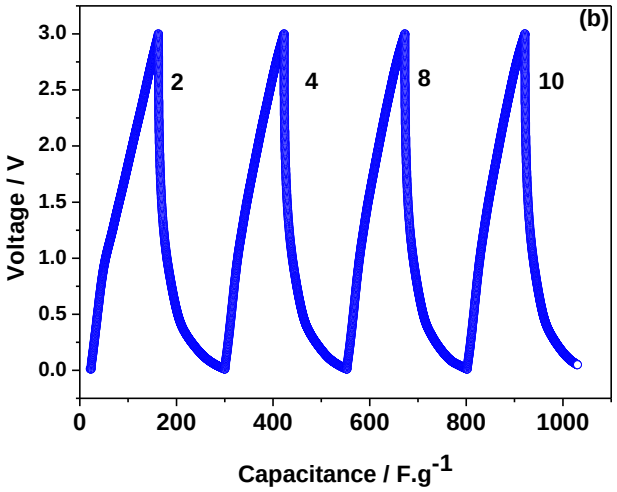

Figure 8. Galvanostatic (charge-discharge) cycling of as-synthesized multi-component olivine $LiMn_{1/3}Co_{1/3}Ni_{1/3}PO_4$ samples with chelating agents (a) PVP, (b) TEA and (c) carbon powder versus metallic lithium in 1M $LiPF_6$ dissolved in ethylene carbonate, diethyl carbonate and dimethyl carbonate (2:1:2 v/v) non-aqueous electrolyte at a current rate of 0.12 A/g. The graphs show an excellent reversibility during the first ten cycles but the available capacitance is higher for (a) PVP than (b) TEA. Cycles numbers are indicated in the figure.

The profiles for the first ten cycles (data shown for alternative cycles) at a constant specific current 0.12 A/g is shown in the Fig. 8. The discharge capacitances of the olivine PVP, TEA and carbon electrodes in the first cycle are 125 F/g, 78 F/g and 134 F/g, while for the tenth cycle are 96 F/g, 53 F/g, and 108 F/g, respectively. The capacitance retention ratio after the tenth cycle of olivine PVP, TEA and carbon is calculated to be 75%, 67% and 80%, respectively. The available capacitance and its retention upon subsequent cycles for $LiMn_{1/3}Co_{1/3}Ni_{1/3}PO_4$ (PVP) and carbon seem to be excellent, demonstrating a highly reversible reaction.

3.2.3 Galvanostatic (charge-discharge) studies: Olivine vs. Carbon (hybrid device)

Figures 9-10 present the potential-time profiles of the $LiMn_{1/3}Co_{1/3}Ni_{1/3}PO_4$ / C hybrid capacitor (combination of battery type olivine and capacitor type carbon) for PVP and TEA respectively.

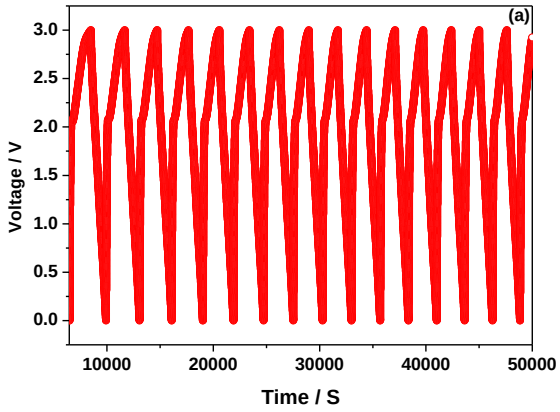

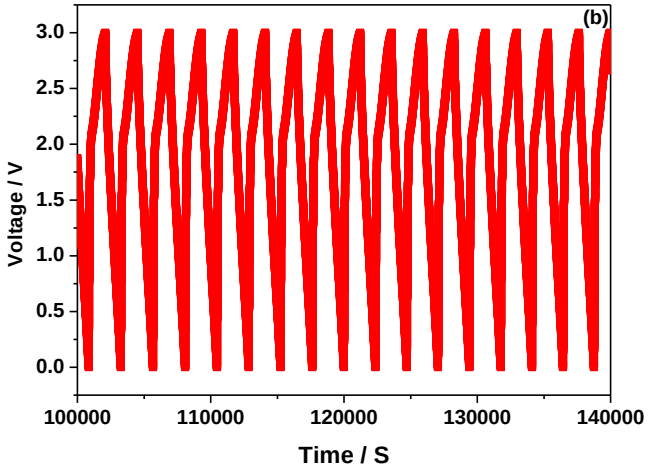

Figure 9. Voltage vs time of as-synthesized multi-component olivine $LiMn_{1/3}Co_{1/3}Ni_{1/3}PO_4$ samples with PVP as chelating versus Carbon (full cell) in 1M $LiPF_6$ dissolved in ethylene carbonate, diethyl carbonate and dimethyl carbonate (2:1:2 v/v) non-aqueous electrolyte at a constant current of 0.12 A/g. The graph (a-b) shows an excellent reversibility and capacitive behaviour even after hundreds of consecutive cycles.

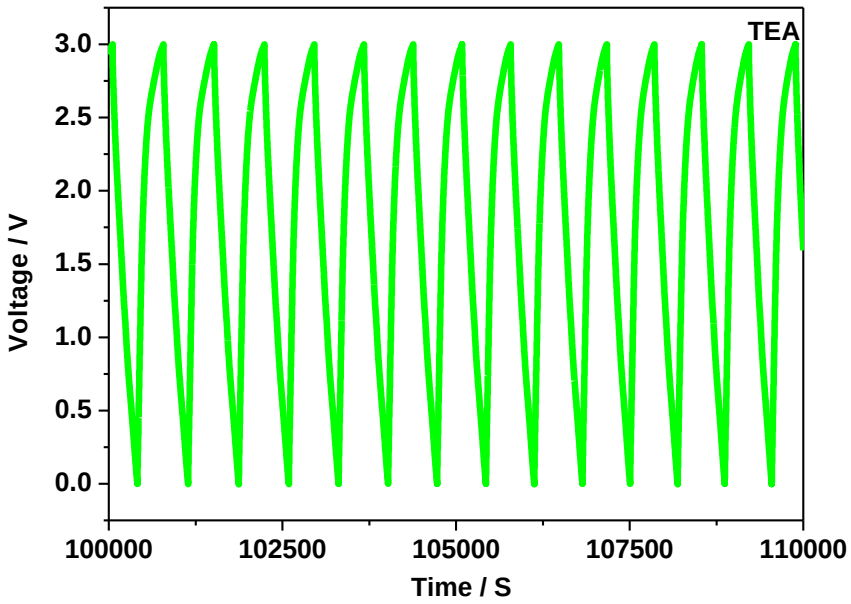

Figure 10. Voltage vs time of as-synthesized multi-component olivine $LiMn_{1/3}Co_{1/3}Ni_{1/3}PO_4$ samples with TEA as chelating versus Carbon (full cell) in 1M $LiPF_6$ dissolved in ethylene carbonate, diethyl carbonate and dimethyl carbonate (2:1:2 v/v) non-aqueous electrolyte at a constant current of 0.12 A/g The graph shows a decreased capacitive behaviour while cycling.

The charge-discharge characteristics of the hybrid cell were investigated by measuring its galvanostatic charge discharge curves in the non-aqueous solutions between the voltage window 0.0 and 3.0 V and the results are displayed in Figures 9-10 for subsequent 250 cycles. The galvanostatic charge-discharge curves tested in coin cells in Fig. 9 exhibit smooth sloping profiles between 0.0 – 2.0

V and a slight plateau like curve is observed between 2.0 – 3.0 V. The plateau like curve could be attributed to pseudocapacitive in nature of the material resulting from the Li^+ de-intercalation and intercalation process [44, 47] as seen in the CV curves (Fig. 7a). This observation is in good agreement with the finding in Fig. 7a, the total capacitance combines the EDL and pseudo-capacitance. The discharge capacitances of the hybrid device for PVP in the 1st, 100th and 250th cycles are 86, 72 and 53 F/g, respectively. While the discharge capacitances for TEA in the 1st, 100th and 250th cycles are 80, 48 and 31 F/g, respectively. The coulombic efficiency of the hybrid device for PVP is above 90% even after 200 cycles. Initially, the efficiency was only 77% and due to the typical behavior of PVP as the chelating agent, trapped organic layer and the polymer matrix enhances the pseudocapacitive behaviour [48] and the efficiency was improved to 90% after 100 cycles and keeps steady thereon. The proposed reaction for the commercial carbon is

$$C + xLi^+ + xe^- \leftrightarrow C^{x-} \,||\, xLi^+ \qquad \text{Eq. [1]}$$

In addition to the proposed Li absorption reaction in eq. (1) electric double layer with the anion, PF_6^- from the electrolyte could not be ruled out. As the chosen commercial carbon is of amorphous in nature (evidenced earlier from the TEM analysis Fig. 5) intercalation of lithium and its structural stability could be less likely. On the basis of extensive electrochemical characterization, the reaction thus proposed for the charge/discharge processes of multi-component olivine cathode is as follows with the mechanism of lithium insertion/extraction.

$$LiMn_{1/3}Co_{1/3}Ni_{1/3}PO_4 \underset{\text{Discharge}}{\overset{\text{charge}}{\rightleftharpoons}} Li_{1-x}Mn_{1/3}Co_{1/3}Ni_{1/3}PO_4 + x\,Li^+ + x\,e^- \qquad \text{Eq. [2]}$$

3.2.4 Cycling and rate capability studies: hybrid device

Figure 11 comparatively depicts the cycling performance of $LiMn_{1/3}Co_{1/3}Ni_{1/3}PO_4$ / C hybrid capacitor for PVP and TEA.

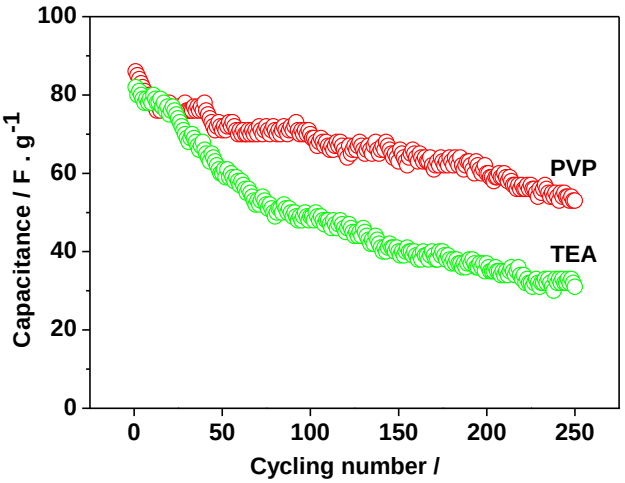

Figure 11. The cycling discharge capacitance as-synthesized multi-component olivine $LiMn_{1/3}Co_{1/3}Ni_{1/3}PO_4$ samples with PVP and TEA as chelating versus Carbon (full cell) in 1M $LiPF_6$ dissolved in ethylene carbonate, diethyl carbonate and dimethyl carbonate (2:1:2 v/v) non-aqueous electrolyte at a constant current of 0.12 A/g.

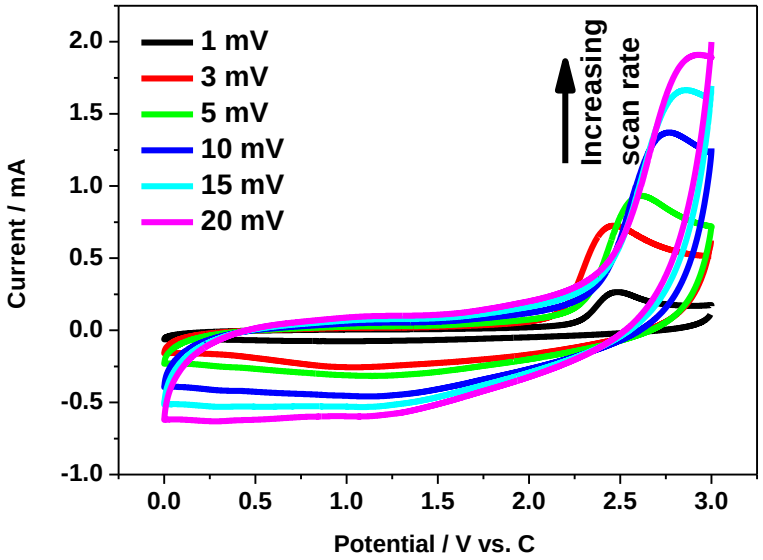

Figure 12. The rate capability behaviour of as-synthesized multi-component olivine $LiMn_{1/3}Co_{1/3}Ni_{1/3}PO_4$ samples with PVP as chelating versus Carbon (full cell) in 1M $LiPF_6$ dissolved in ethylene carbonate, diethyl carbonate and dimethyl carbonate (2:1:2 v/v) non-aqueous electrolyte at different sweep rate noted in the legend.

The PVP hybrid shows a much higher capacitance, better capacitance retention of 62% of the first discharge capacitance (from 86 F/g to 53 F/g), more superior coulombic efficiency of 90% from 100 cycle onwards and its cyclability stabilising thereon. Although the initial capacitance for TEA is quite high but it decreases gradually upon successive cycling and the retention of capacitance is only 31 F/g after 250 cycles this could be due to the nature of the chelating agent or may be originated from the reduction of electrode integrity. The PVP and TEA hybrid cell exhibits energy densities of 75 and 25 Wh/kg at power densities of 180 W/kg, respectively. The energy density (E) and power density (P) are calculated using the relations, $P = (\Delta E \cdot I / m)$ and $E = (P \cdot t / 3600)$ where $\Delta E = ((E_{max}$ (end of charge potential) + E_{min} (end of discharge potential)) /2, *t* the time for charge/discharge, *I* the applied current and *m* the weight of active material in the electrode [49]. Figure 12 shows the CV plots of hybrid capacitor at different scan rates (1 – 20 mV/s) between 0 – 3.0 V potential window. At a higher scan rate i.e. $\geq$ 15 mV/s the oxidation peaks are ill-defined. The peak potential difference between the two peaks increased dramatically at the high scan rate implying a slow electron transfer [50-51]. Increasing the scan rate increases the lithium ion charge-discharge kinetics than the lithium ion diffusion in the bulk resulting in decreased specific capacitance. The improved cycle stability and high rate performance for PVP sample could be attributed to the high contact area between electrolyte and electrode of the hybrid, polymer matrix preventing the agglomeration of particles and allow sufficient infiltration of electrolyte.

4. CONCLUSIONS

In summary, we developed a combination of Mn, Co and Ni i.e. multi-component olivine phosphate ($LiMn_{1/3}Co_{1/3}Ni_{1/3}PO_4$) vs. carbon for hybrid capacitor applications. Nanocomposites of

olivine were synthesized by sol-gel method using PVP and TEA chelating agents. Microscopy images confirm that chelating agents had a key role on the particle shape, size, pore size distribution, morphology and particle aggregation. The PVP sample showed excellent coulombic efficiency (90%) and good capacitance retention (62% after 250 cycles) over TEA sample. The trapped organic species in the electrode-electrolyte interface for the PVP sample enhances the rate of lithium ion diffusion with better electrochemical performance. Significantly, the concept of mixed transition metal cations based on an olivine lithium phosphate has been proposed for the first time, which may facilitate the application of olivine //carbon as feasible electrodes for hybrid capacitors.

ACKNOWLEDGEMENTS

The author (M. M) wishes to acknowledge the funding bodies, Australia-India Strategic Research Fund (AISRF) and Australian Research Council (ARC). This research was supported under Australian Research Council (ARC) Discovery Project funding scheme DP1092543 and Australia-India Early Career Research Fellowship. Murdoch University assisted in meeting the publication costs of this article.

References

1. M. Jayalakshmi and K. Balasubramanian, *Int. J. Electrochem. Sci*., 3 (2008) 1196.
2. P. Simon and Y. Gogotsi, *Nat. Mater*. 7 (2008) 845.
3. H. Ji, X. Zhao, Z. Qiao, J. Jung, Y. Zhu, Y. Lu, L. L. Zhang, A.H. MacDonald and R. S. Ruoff, *Nat. Commun*. 5 (2014) 3317.
4. B.E. Conway, V. Birss, and J. Wojtowicz, *J. Power Sources* 66 (1977) 1.
5. B. E. Conway and W. G. Pell, *J. Solid State Electrochem*. 7 (2003) 637.
6. R. J. Brodd, K. R. Bullock, R. A. Leising, R. L. Middaugh, J. R. Miller and E. Takeuchi, *J. Electrochem. Soc*., 151 (2004) K1.
7. S. Fiorenti, J. Guanetti, Y. Guezennec and S.Onori, *J. Power Sources* 241 (2013) 112.
8. Y.X. Gu, D. R. Chen and X. L. Jiao, *J. Phys. Chem*. B 109 (2005) 17901.
9. E. Hosono, T. Kudo, I. Honma, H. Matsuda and H.S. Zhou, *Nano Lett*. 9 (2009) 1045.
10. A. K. Padhi, K. S. Nanjundaswamy, C. Masquelier, S. Okada and J. B. Goodenough, *J. Electrochem. Soc*. 144 (1997) 1609.
11. A. V. Murugan, T. Muraliganth, P. J. Ferreira and A. Manthiram, *Inorg. Chem*. 48 (2009) 946.
12. S. L. Chou, J. Z. Wang, J. Z. Sun, D. Wexler, M. Forsyth, H. K. Liu, D. R. MacFarlane and S. X. Dou, *Chem. Mater*. 20 (2008) 7044.
13. C. Niu, E. K. Sichel, R. Hoch, D. Moy and H. Tennent, *Appl. Phys. Lett*. 70 (1997) 1480.
14. N. Wang, H. Pang, H. Peng, G. Li and X. Chen, *Cryst. Res. Technol*. 44 (2009) 1230.
15. X. Tang, H. Li, Z. H. Liu, Z. Yang and Z. Wang, *J. Power Sources* 196 (2011) 855.
16. J. Xu, L. Gao, J. Cao, W. Wang, and Z. Chen, *Electrochim. Acta* 56 (2010) 732.
17. C. Kim, K. S. Yang and W. J. Lee, *Electrochem. Solid State Lett*. 7 (2004) A397.
18. K. Naoi, *Fuel Cells* 10 (2010) 825.
19. D. Cericola, and R. Kotz, *Electrochim. Acta* 72 (2012) 1.
20. A. D. Fabio, A. Giorgi, M. Mastragostino, and F. Soavi, *J. Electrochem. Soc*. 148 (2001) A845.
21. A. D. Pasquier, A. Laforgue, and P. Simon, *J. Power Sources* 125 (2004) 95.
22. A. M. Glushenkov, D. Hulicova-Jurcakova, D. Llewellyn, G. Q. Lu and Y. Chen, *Chem. Mater*. 22 (2010) 914.
23. G.G. Amatucci, F. Badway, A.D. Pasquier, and T. Zheng, *J. Electrochem. Soc*., 148 (2001) A930.

24. V. Aravindan, M. V. Reddy, S. Madhavi, S.G. Mhaisalkar, G. V. Subbarao, B. V. R. Chowdari, *J. Power Sources* 196 (2011) 8850.
25. R. Vasanthi, D. Kalpana, and N. G. Renganathan, *J. Solid State Electrchem*. 12 (2008) 961.
26. F. Zhou, M. Cococcioni, K. Kang, and G. Ceder, *Electrochem. Commun*. 6 (2004) 1144.
27. J. Wolfenstine and J. Allen, *J. Power Sources* 142 (2005) 389.
28. S. Kandhasamy, A. Pandey, and M. Minakshi, *Electrochim. Acta* 60 (2012) 170.
29. H. Gwon, D.-H. Seo, S. –W. Kim, J. Kim and K. Kang, *Adv. Fun. Mater*., 19 (2009) 3285.
30. N. Ding, X. W. Ge and C. H. Chen, *Mater. Res. Bull*. 40 (2005) 1451.
31. L. J. Fu, H. Liu, C. Li, Y.P. Wu, E. Rahm, R. Holze and H.Q. Wu, *Progress in Mater. Sci*. 50 (2005) 881.
32. S. G. Kang, S. Y. Kang, K. S. Ryu and S. H. Chang, *Solid State Ionics* 120 (1999) 155.
33. A. K. Padhi, K. S. Nanjundaswamy, and J. B. Goodenough, *J. Electrochem. Soc*. 144 (1997) 1188.
34. R. S. Okojie, T. Holzheu, X.R. Huang and M. Dudley, *Appl. Phys. Lett*. 83 (2003) 1971.
35. T. Nagasaki, K. Kok, A.H. Yahaya, N. Igawa, K. Noda and H. Ohno, *Solid State Ionics* 96 (1997) 61.
36. T. Sugimoto, X. Zhou and A. Muramatsu, *J. Colloidal and Interface Sci*. 259 (2003) 43.
37. S. Lim and J. Cho, *Electrochem. Commun*. 10 (2008) 1478.
38. W. Li, G. Zheng, Y. Yang, Z. W. She, N. Liu, and Y. Cui, *PNAS* 110 (2013) 7148.
39. M. W. Pitcher, Y. He, and P. A. Bianconi, *Mater. Chem and Phys.* 90 (2005) 57.
40. O. Barbieri, M. Hahn, A. Herzog and R. Kotz, *Carbon* 43 (2005) 1303.
41. H. Itoi, H. Nishihara, T. Kogure and T. Kyotani, *J. Am. Chem. Soc*., 133 (2011) 1165.
42. L. Eliad, E. Pollak, N. Levy, G. Salitra, A. Soffer and D. Aurbach, *Appl. Phys*. A 82 (2006) 607.
43. K. Amine, H. Yasuda, and M. Yamachi, *Electrochem. Solid State Lett*. 3 (2000) 178.
44. B. E. Conway and W. G. Pell, *J. Solid State Electrochem*. 7 (2003) 637.
45. R. N. Reddy and R. G. Reddy, *J. Power Sources* 124 (2003) 330.
46. B. E. Conway, Electrochemical supercapacitors: scientific fundamentals and technological applications: Kluwer/Plenum, New York (1999).
47. H. D. Yoo, E. Markevich, G. Salitra, D. Sharon and D. Aurbach, *Mater. Today*. 17 (2014) 110.
48. K. S. Park, S. B. Schougaard, and J. B. Goodenough, *Adv. Mater*. 19 (2007) 848.
49. T. Cottineau, M. Toupin, T. Delahaye, T. Brousse and D. Belanger, *Appl. Phys*. A, 82 (2006) 599.
50. N. Li, C. J. Patrissi, G. Che, and C. R. Martin, *J. Electrohem. Soc*., 147 (2000) 2044.
51. M. D. Levi, and D. Aurbach, *J. Electronal. Chem*. 421 (1997) 79.